Nanoscale

ROYAL SOCIETY OF CHEMISTRY

PAPER

View Article Online
View Journal | View Issue

Check for updates

Cite this: *Nanoscale*, 2020, **12**, 1958

# Remarkable quality improvement of as-grown monolayer $MoS_2$ by sulfur vapor pretreatment of $SiO_2$/Si substrates†

Peng Yang,[a] Yabing Shan,[a] Jing Chen,[a] Garel Ekoya,[a] Jinkun Han,[a] Zhi-Jun Qiu,[a] Junjie Sun,[b] Fei Chen,[b] Haomin Wang,[c] Wenzhong Bao,[d] Laigui Hu,[a] Rong-Jun Zhang,[a] Ran Liu[a] and Chunxiao Cong *[a,e]

Received 25th October 2019,
Accepted 19th December 2019

DOI: 10.1039/c9nr09129g

rsc.li/nanoscale

Monolayer $MoS_2$ is a direct bandgap semiconductor which is believed to be one of the most promising candidates for optoelectronic devices. Chemical vapor deposition (CVD) is the most popular method to synthesize monolayer $MoS_2$ with a large area. However, many defects are always found in monolayer $MoS_2$ grown by CVD, such as sulfur vacancies, which severely degrade the performance of devices. This work demonstrates a concise and effective method for direct growth of high quality monolayer $MoS_2$ by using $SiO_2$/Si substrates pretreated with sulfur vapor. The $MoS_2$ monolayer obtained using this method shows about 20 times PL intensity enhancement and a much narrower PL peak width than that grown on untreated substrates. Detailed characterization studies reveal that $MoS_2$ grown on sulfur vapor pretreated $SiO_2$/Si substrates has a much lower density of sulfur vacancies. The synthesis of monolayer $MoS_2$ with high optical quality and low defect concentration is critical for both fundamental physics studies and potential practical device applications in the atomically thin limit.

## Introduction

Atomically thin two-dimensional transition metal dichalcogenides (TMDCs) have attracted tremendous attention due to their remarkable optical and electrical properties, which make them promising candidates for use in next-generation semiconductors.[1–8] As a typical member of TMDCs, $MoS_2$ has been intensively studied. $MoS_2$ transits from an indirect-to-direct bandgap when the material is thinned from bulk to a monolayer.[9,10] As a consequence, photoluminescence (PL) arising from the direct bandgap in monolayer $MoS_2$ broadens its application in optoelectronics such as photovoltaics, photodetectors, light sensors and light emitters.[11–14] Many researchers have focused on the synthesis of the $MoS_2$ monolayer on a wafer scale and improvement of the optical and electrical performance to speed up its practical applications.[2,15–19] It has been demonstrated that chemical vapor deposition (CVD) is the most popular fabrication technique for synthesizing large-area monolayer $MoS_2$ films.[16–19] However, the structural defects in CVD $MoS_2$, such as the most commonly seen sulfur vacancies, limit its application in high-performance nanoelectronic and optoelectronic devices.[20–23] To overcome this challenge, many attempts have been made to repair the chalcogen vacancies in $MoS_2$, such as post-treatment of $MoS_2$ with organic reagents which contain sulfur bonded functional groups, oxygen bonding through plasma irradiation on the surface of $MoS_2$, and so on.[23–30] Near-unity photoluminescence quantum yield in mechanically exfoliated monolayer $MoS_2$ has been achieved by treatment with an organic superacid,[26] and was assumed to repair the sulfur vacancies in $MoS_2$.[23] Such a post-treatment process will introduce other unwanted organic impurities on the surface of $MoS_2$,[28] which thus even act as trap sites and further degrade the properties of $MoS_2$ devices leading to their poor electrical performances.[27,31] In all, a method to grow monolayer $MoS_2$ with fewer structural defects is highly desired.

Here, we report a simple but effective method to obtain high quality monolayer $MoS_2$ through sulfur vapor pretreatment of $SiO_2$/Si substrates. The differences between monolayer

[a]State Key Laboratory of ASIC and System, School of Information Science and Technology, Fudan University, Shanghai 200433, China.
E-mail: cxcong@fudan.edu.cn
[b]State Key Laboratory of Laser Interaction with Matter, Innovation Laboratory of Electro-Optical Countermeasures Technology, Changchun Institute of Optics, Fine Mechanics and Physics, Chinese Academy of Sciences, 3888 Dongnanhu Road, Changchun Jilin 130033, China
[c]State Key Laboratory of Functional Materials for Informatics, Shanghai Institute of Microsystem and Information Technology, Chinese Academy of Sciences, Changning Road 865, Shanghai 200050, China
[d]State Key Laboratory of ASIC and System, School of Microelectronics, Fudan University, Shanghai 200433, China
[e]Academy for Engineering and Technology, Fudan University, Shanghai 200433, China

†Electronic supplementary information (ESI) available. See DOI: 10.1039/c9nr09129g

$MoS_2$ grown on sulfur vapor pretreated $SiO_2$/Si substrates and that grown on untreated $SiO_2$/Si substrates were systematically investigated. A series of characterization studies including photoluminescence spectroscopy, Raman spectroscopy, X-ray photoelectron spectroscopy (XPS), and electrical transport measurements were carried out to evaluate the quality of the as-grown $MoS_2$ samples. Through systematical comparison, all the results indicate that monolayer $MoS_2$ grown on the sulfur vapor pretreated $SiO_2$/Si substrate has a much lower density of sulfur vacancies. About 20 times enhancement in the PL intensity as well as better electrical performance was observed in monolayer $MoS_2$ grown on sulfur vapor pretreated $SiO_2$/Si substrates than that grown on untreated substrates. The strategy of synthesizing monolayer $MoS_2$ by sulfur vapor pretreatment of $SiO_2$/Si substrates is not only beneficial to greatly improve the quality of as-grown monolayer $MoS_2$, but also compatible to the existing mature process of planar semiconductor devices. This pretreatment strategy can avoid the unwanted defects and impurities which may be introduced during post-treating process by organic reagents. Our method demonstrated here will benefit the research community in the synthesis of high quality monolayer $MoS_2$ and its further application.

## Experimental

### Sulfur vapor pretreatment of $SiO_2$/Si substrates

A two-temperature-zone heating furnace with a 2-inch quartz tube was used for both treating the growth substrates in a sulfur vapor environment and synthesizing monolayer $MoS_2$. The temperature of the two-heating zones can be independently controlled during the whole process. A high purity sulfur slice (Aladdin, 99.9%) and $SiO_2$/Si substrates (300 nm $SiO_2$) were separately loaded in a one-end sealed quartz tube and fixed at the center of the corresponding heating zone, which could effectively increase the concentration and pressure of sulfur vapor during the pretreatment of the substrates. Next, the sulfur source was heated to 200 °C to produce sulfur vapor. The $SiO_2$/Si substrates were pretreated at 200 °C, 400 °C, 500 °C, 600 °C, and 700 °C individually for an hour in the sulfur vapor environment. After the pretreated $SiO_2$/Si substrates were cooled down to room temperature, several droplets of perylene-3,4,9,10-tetracarboxylic acid tetrapotassium salt (PTAS) solution were dropped on the pretreated $SiO_2$/Si substrates. The $MoS_2$ samples were synthesized by using home-made CVD equipment with $MoO_3$ powder and sublimed sulfur as the growth source, and the growth temperature was set at 680 °C using high purity Ar as the carrier gas under atmospheric pressure. The details about growth recipe can be found in our previous publication.[19]

### Characterization studies

The optical images were acquired using optical microscopy (Keyence digital microscope VHX-600). Raman mapping and PL mapping were carried out using a confocal Raman microscope (WITec Alpha 300R) with a 532 nm laser for the excitation. The Raman signal was collected using a 100× (Zeiss, N.A. = 0.9) objective lens after being dispersed by optical grating (1800 lines per mm); the same measurement parameters were chosen for the PL measurement, but 150 lines per mm was chosen. To avoid the heating effect, the power of the excitation laser was kept at 0.5 mW. All the Raman and PL measurements except temperature dependent PL were carried out at room temperature in air. The temperature dependent PL spectra were recorded using confocal micro-Raman spectroscopy (Renishaw) with a 514 nm laser for the excitation through a 50× (Leica, N.A. = 0.5) objective lens after being dispersed by optical grating (1800 lines per mm) in a Linkam thermal stage. The extended grating scan type was chosen to obtain PL spectra in the selected range, and the laser power was kept below 0.1 mW to ultimately avoid the heating effect. The XPS spectra were recorded using a ThermoFisher ESCALAB 250Xi with an Al Kα X-ray source under a pressure of $2.2 \times 10^{-10}$ mbar.

### TFSI treatment of $MoS_2$

The treatment process of our CVD grown monolayer $MoS_2$ with bis(trifluoromethane)sulfonimide (TFSI) is as follows: 100 mg TFSI (Aladdin) was dissolved in 500 mL dichloromethane ($CH_2Cl_2$) to make a 0.2 mg $ml^{-1}$ TFSI solution, and then the monolayer $MoS_2$ samples grown on $SiO_2$/Si substrates were immersed in 10 ml TFSI solution in a tightly closed vial, and then the vial was placed on a heated hotplate at 100 °C for 10 min. After the vial was cooled down to room temperature, the samples were subsequently taken out and placed on the hotplate (100 °C) for 5 min and finally cooled down to room temperature.

### Fabrication and testing of $MoS_2$ FET devices

Two electrodes (source/drain) were patterned by photolithography using a laser direct writing machine (MicroWriter ML③3) without a photomask. 5 nm Cr and 50 nm Au were deposited by thermal evaporation (Kurt J. Lesker, NANO 36) as the metal electrodes for making $MoS_2$ field effect transistors (FETs). Then the devices were annealed under 190 sccm Ar and 10 sccm $H_2$ at 200 °C for 2 h to remove the organic residuals and improve the contact between the $MoS_2$ sample and metal electrodes. All the electrical measurements were carried out using an Agilent Technologies B1500A semiconductor device analyzer under dark conditions at room temperature in an ambient atmosphere.

## Results and discussion

Fig. 1(a) shows the schematic of the experimental setup for pretreating $SiO_2$/Si substrates in a sulfur vapor environment. The extremely enhanced PL of monolayer $MoS_2$ can be found when the $SiO_2$/Si substrates were pretreated with sulfur vapor at 600 °C (if not specified, all the pretreatments of the $SiO_2$/Si substrates are carried out at 600 °C in a sulfur vapor environment; the details are discussed later). As shown in Fig. 1(b)

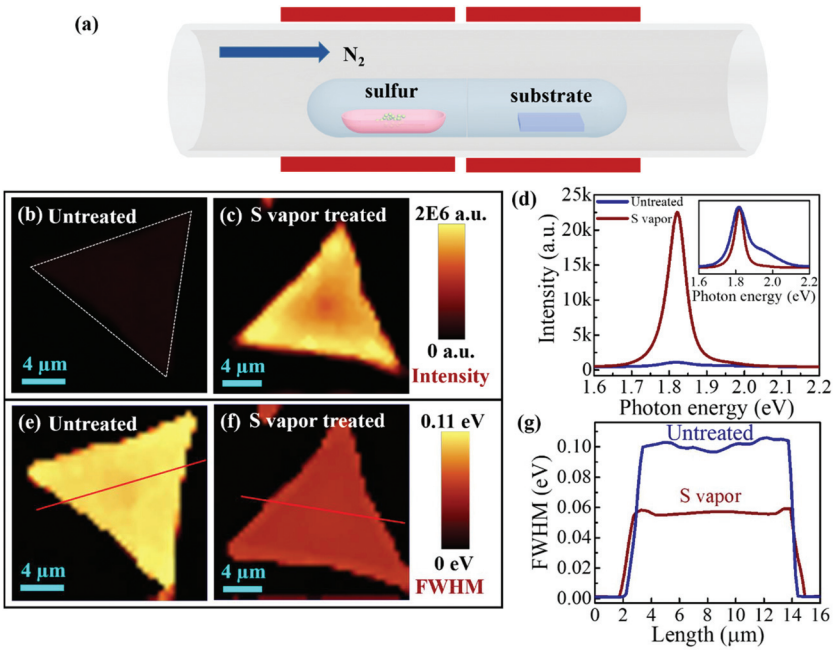


**Fig. 1** (a) Schematic of the experimental setup for pretreating $SiO_2$/Si substrates in sulfur vapor. (b and c) PL peak intensity mapping of CVD grown monolayer $MoS_2$ on untreated (b) and sulfur vapor pretreated $SiO_2$/Si substrates (c). (d) Typical PL spectra of $MoS_2$ grown on untreated (blue line) and sulfur vapor pretreated $SiO_2$/Si substrates (red line). The inset shows the normalized PL spectra. (e and f) PL mapping of full width at half maximum (FWHM) of $MoS_2$ domains corresponding to (b and c), respectively. (g) PL peak linewidth corresponding to the red line in (e and f).

and (c), the PL intensity of the whole monolayer $MoS_2$ flake grown on the sulfur pretreated $SiO_2$/Si substrate was about 20 times higher than that grown on the untreated $SiO_2$/Si substrate, which can be due to the much more defect-mediated nonradiative recombination existing in $MoS_2$ grown on the untreated substrate.[32] The representative extracted PL spectra from the PL mapping of monolayer $MoS_2$ grown on sulfur vapor pretreated and untreated substrates are shown in Fig. 1(d). A narrower linewidth is observed in $MoS_2$ grown on sulfur vapor pretreated substrates as seen from the inset of Fig. 1(d). Such an extremely enhanced PL with a narrow linewidth of monolayer $MoS_2$ grown on the sulfur vapor pretreated substrate indicates the much better optical quality of monolayer $MoS_2$ grown on the sulfur vapor pretreated substrate than that grown on the untreated substrate.[23,25,26] Due to the spin–orbit splitting of the highest valence band, there are two direct-gap emission peaks called A-excitons and B-excitons in the PL spectrum of monolayer $MoS_2$.[9] It has been reported recently that the A- and B-exciton photoluminescence intensity ratio can be used to measure the sample quality for transition metal dichalcogenide monolayers such as $MoS_2$, $MoSe_2$, $WS_2$, and $WSe_2$.[33] The A- and B-excitons are easily seen in $MoS_2$ grown on the untreated $SiO_2$/Si substrate, whereas the B-excitons in $MoS_2$ grown on the sulfur vapor pretreated substrate are not so easy to discern because of the remarkably high intensity of A-excitons. Upon further analysis and re-plotting the same PL spectra, as shown in Fig. 1(d), with intensity on a log-scale, the B-excitons become discernible, as shown in Fig. S1.† The intensity ratios of B-excitons *versus* A-excitons (B/A) are about 1/2 and 1/20 in $MoS_2$ grown on untreated and sulfur vapor pretreated substrates, respectively. Therefore, we can qualitatively assess the quality of $MoS_2$ samples through the B/A ratio; a low B/A ratio in $MoS_2$ grown on the sulfur vapor pretreated $SiO_2$/Si substrate indicates low defect density and thus corresponds to high crystalline quality. For comparison, we also recorded the PL spectra and mapping of mechanically exfoliated monolayer $MoS_2$ (shown in Fig. S2†). The PL intensity of monolayer $MoS_2$ grown on untreated substrates has the same magnitude as that of the exfoliated monolayer $MoS_2$, which means that the PL intensity of monolayer $MoS_2$ grown on pretreated substrates is much stronger than that of exfoliated monolayer $MoS_2$, that is, the optical quality of monolayer $MoS_2$ grown on the pretreated substrate is much better than that of mechanically exfoliated monolayer $MoS_2$. We show the PL mapping of full width at half maximum (FWHM) and the corresponding linewidth in Fig. 1(e–g). It can be found that the FWHM of $MoS_2$ grown on sulfur vapor pretreated substrates is only a half of that of $MoS_2$ grown on the untreated substrate, which means less structural disorder or defects and better crystallinity in the former. The PL peak width of as-grown monolayer $MoS_2$ (50–60 meV) on the sulfur vapor pretreated substrate is comparable to that of the CVD grown sample on h-BN and free-standing $MoS_2$.[9,34–36] These characteristics of PL suggest that the $MoS_2$ grown on the sulfur vapor pretreated $SiO_2$/Si substrate is less perturbed due to its high quality.[36,37]

To further evaluate the quality of $MoS_2$ flakes, we carried out temperature dependent PL characterization. As shown in

 

Fig. S3,† for the monolayer $MoS_2$ grown on untreated substrates, a shoulder peak below the A exciton starts appearing when the temperature is decreased to 140 K, and the relative intensity of this peak increases with a further decrease in temperature, whereas for the monolayer $MoS_2$ sample grown on the sulfur vapor pretreated substrate, this shoulder peak only appears when the temperature is decreased to 100 K. It is obvious that the relative intensity of this shoulder peak to A exciton is much weaker than that of $MoS_2$ on the untreated substrate at the same temperature. This shoulder peak is denoted as localized states (L peak) probably originating from defects, impurities, and disorders, and is also found in other TMDCs such as $WS_2$.[38,39] It was believed that the L peak is related to defect-bound excitons such as sulfur vacancies in $MoS_2$ and $WS_2$.[38–41] Combining the extremely enhanced PL and the relatively weaker L peak that emerged at low temperature, we assume that a much lower density of sulfur vacancies exists in $MoS_2$ grown on the sulfur vapor pretreated substrate than on the untreated substrate.

Raman characterization was performed to further investigate the crystal quality of the $MoS_2$ flakes grown on the $SiO_2$/Si substrate with and without sulfur vapor pretreatment, as shown in Fig. 2. The typical Raman spectrum of $MoS_2$ grown on the untreated substrate, shown in the top panel of Fig. 2(a), exhibits two characteristic peaks at 383.6 $cm^{-1}$ and 403.4 $cm^{-1}$ corresponding to the in-plane vibration $E_{2g}{}^1$ mode and out-of-plane vibration $A_{1g}$ mode. The peak difference between the two modes is 19.8 $cm^{-1}$, indicating the monolayer characteristic of the CVD synthesized $MoS_2$.[5,21–23] It is known that the in-plane $E_{2g}{}^1$ mode of $MoS_2$ is sensitive to strain and the out-of-plane $A_{1g}$ mode is related to doping.[42] For the Raman spectrum of monolayer $MoS_2$ grown on the sulfur vapor pretreated substrate in the lower panel of Fig. 2(a), the in-plane $E_{2g}{}^1$ mode shows a 0.7 $cm^{-1}$ shift towards lower wavenumbers compared with $MoS_2$ grown on the untreated substrate. This obvious red shift of the $E_{2g}{}^1$ mode is assumed to be due to the reduced sulfur vacancies, which lead to the release of compress strain.[23,43] The blue shift in the $A_{1g}$ mode suggests that the reduced n-doping is induced by the much lower density of sulfur vacancy defects.[23,42] The red shift of the $E_{2g}{}^1$ mode and the blue shift of the $A_{1g}$ mode are observed in the whole flake of monolayer $MoS_2$ grown on the sulfur vapor pretreated substrate from the Raman peak position mapping, as shown in Fig. 2(b–e); the statistic peak positions of the $E_{2g}{}^1$ mode and $A_{1g}$ mode are also shown in Fig. S4.† In addition, we find that the Raman mapping of the FWHM of the $E_{2g}{}^1$ mode does not show an obvious difference in $MoS_2$ grown on both substrates, whereas the FWHM of the $A_{1g}$ mode in monolayer $MoS_2$ grown on the sulfur vapor pretreated substrate is slightly narrower than that grown on the untreated substrate, as shown in Fig. S5.† The FWHM value of the $A_{1g}$ mode in monolayer $MoS_2$ grown on the sulfur vapor pretreated substrate is about 4.5 $cm^{-1}$, which is even narrower compared to that of the $MoS_2$ grown on h-BN,[44] indicating the reduced electron–phonon coupling related to structural disorder and doping in $MoS_2$ grown on the sulfur vapor pretreated substrate.[42] Furthermore, we carried out XPS measurements on $MoS_2$ grown on sulfur vapor pretreated and untreated substrates. As shown in Fig. S6,† the Mo 3d core level spectra were fitted with three sets of double peaks corresponding to three kinds of Mo bonded compound states. The purple curve with double peaks located at 236.1 and 232.9 eV represents $Mo^{6+}$ $3d_{3/2}$ and $3d_{5/2}$ doublets of $MoO_3$ or $MoO_x$, respectively, which may be attributed to the residual growth source that was incompletely sulfurized.[45] The $Mo^{4+}$ spectra were deconvoluted into two components, for the green doublets corresponding to $Mo^{4+}$ $3d_{3/2}$ and $3d_{5/2}$ in stoichiometric intrinsic $MoS_2$ (i-$MoS_2$), whereas the blue doublets located at a slightly lower binding energy than green doublets correspond to $Mo^{4+}$ $3d_{3/2}$ and $3d_{5/2}$ in defective $MoS_2$ (d-$MoS_2$) with sulfur vacancies.[23,29,45] Based on this point, from the deconvoluted component spectra in $Mo^{4+}$, it is found that the proportion of d-$MoS_2$ becomes much less

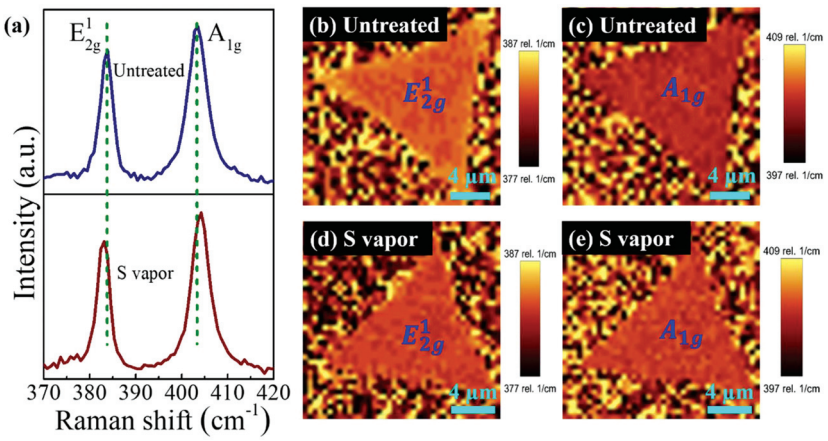


Fig. 2 (a) Typical Raman spectra of monolayer $MoS_2$ grown on the untreated $SiO_2$/Si substrate (blue line) and the sulfur vapor pretreated $SiO_2$/Si substrate (red line). (b and c) Raman peak position mapping of the $E_{2g}{}^1$ mode (b) and $A_{1g}$ mode (c) of monolayer $MoS_2$ grown on the untreated $SiO_2$/Si substrate. (d, e) Raman peak position mapping of the $E_{2g}{}^1$ mode (d) and $A_{1g}$ mode (e) of monolayer $MoS_2$ grown on the sulfur vapor pretreated $SiO_2$/Si substrate.

prominent in $MoS_2$ grown on sulfur vapor pretreated substrates, suggesting reduced sulfur vacancies, further supporting our previous assumption.

To understand the mechanism of reduced sulfur vacancies in as-grown monolayer $MoS_2$ by sulfur vapor pretreatment of $SiO_2$/Si substrates, XPS measurements were performed on the $SiO_2$/Si substrates pretreated with sulfur vapor at different temperatures. Fig. 3(a) and (b) show the XPS spectra of the Si 2s and S 2p core level of $SiO_2$/Si substrates pretreated with sulfur vapor at different temperatures, respectively. It can be seen that below 400 °C, there was no XPS signal of the S element. When the treating temperature exceeds 500 °C, the content of the S element increases with an increase in the treating temperature. It should be noted that before the XPS measurements, the sulfur vapor pretreated substrates were loaded under a pressure of $2.2 \times 10^{-10}$ mbar for more than an hour in order to eliminate the elemental sulfur. So the S 2p core level peak of XPS spectra is ascribed to sulfur related chemical bonds with the terminal atoms on the surface of $SiO_2$/Si substrates. As there are abundant oxygen and silicon dangling bonds on the substrate, sulfur related bonds are the complex of S–O and S–Si bonds, which are similar to the sulfur-terminated chemical bonds on the Si surface.[46–49] From the statistics of the PL spectra of $MoS_2$ grown on sulfur vapor pretreated substrates with different treating temperatures, it is interestingly found that the PL intensity becomes saturated when the treating temperature is beyond 600 °C. The above phenomenon can be explained as follows: at low temperature, no sulfur related chemical bond has been formed yet, so there was almost no obvious difference in the PL intensity when $MoS_2$ was grown on sulfur vapor pretreated substrates below 400 °C. With a further increase in the temperature beyond 500 °C, sulfur related chemical bonds started to form on the surface of the $SiO_2$/Si substrates. The growth period of $MoS_2$ involves the dissociation of the sulfur related chemical bond on the surface of the substrates and the formation of the Mo–S bond at the sulfur vacancies, which is similar to the repair process in the chemical treatment of $MoS_2$.[23,24,28,29] With a further increase in the treating temperature beyond 600 °C, the PL intensity of $MoS_2$ grown on the substrates becomes slightly lower, which may be due to the substitution of the Mo atoms by excess sulfur atoms, leading to other kinds of defects such as antisite defects in the grown $MoS_2$.[20]

Low quantum yields (QYs) in monolayer TMDCs limit their practical application in optoelectronics, which are mainly due to the structural defects in TMDCs. Among all the types of structural defects, chalcogen vacancies are one of the most commonly seen structural defects due to the lowest formation energy.[20,23,41] Eliminating the structural defects such as sulfur vacancies in TMDCs to increase the optical and electrical performance has been widely investigated.[23–30] It is believed that the sulfur vacancies in $MoS_2$ can be repaired by the bis(trifluoromethane)sulfonimide (TFSI) treatment.[23,25,26] Fig. 4 shows the PL mapping and extracted single spectrum of $MoS_2$ grown on untreated and sulfur vapor pretreated substrates before and after TFSI treatment. As for the $MoS_2$ grown on

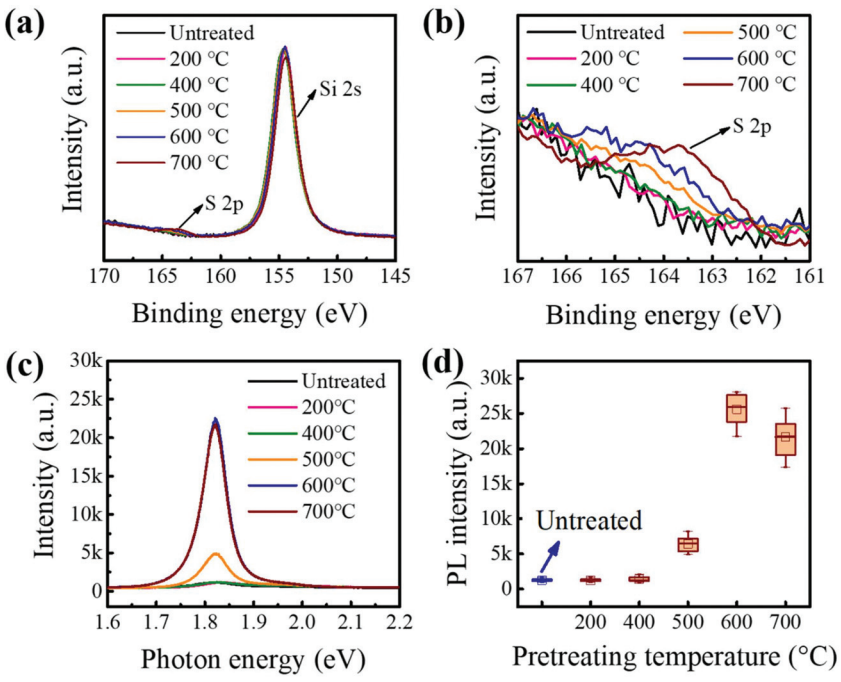


Fig. 3 Investigation of the $SiO_2$/Si substrates treated under different conditions and $MoS_2$ subsequently obtained. (a) XPS spectra of Si 2s and S 2p core level peaks of $SiO_2$/Si substrates pretreated with sulfur vapor at different temperatures. (b) The enlarged S 2p core level spectra of these $SiO_2$/Si substrates. (c) Typical PL spectra of $MoS_2$ grown on $SiO_2$/Si substrates treated with S vapor at different temperatures. (d) Statistics of PL intensities of $MoS_2$ grown on these $SiO_2$/Si substrates.

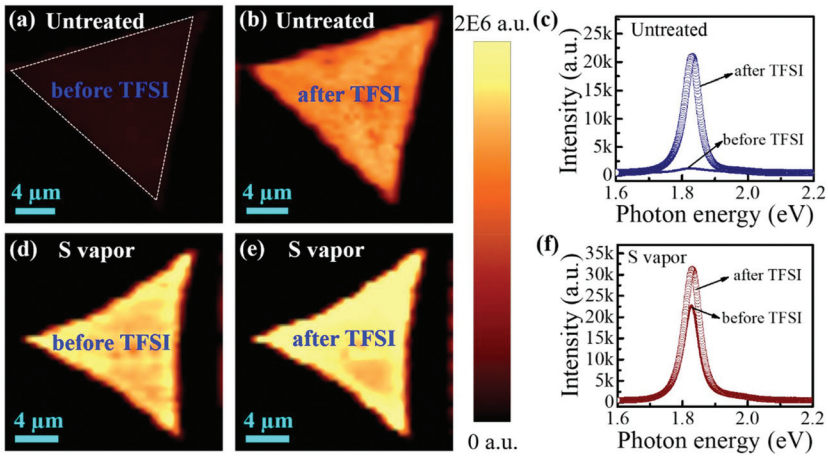


**Fig. 4** (a and b) PL peak intensity mapping of monolayer $MoS_2$ grown on the untreated $SiO_2$/Si substrate before (a) and after TFSI treatment (b). (c) Typical extracted PL spectra from the mapping area of (a, b). (d, e) PL peak intensity mapping of monolayer $MoS_2$ grown on the sulfur vapor pretreated $SiO_2$/Si substrate before (d) and after TFSI treatment (e). (f) Typical extracted PL spectra from the mapping area of (d, e).

untreated substrates, the PL intensity increased about 10 times after TFSI treatment, which means that many sulfur vacancies were repaired by the extrinsic sulfur atoms dissociated from TFSI.[23] And the linewidth of the PL spectrum becomes much narrower, which was assumed to be due to the decreased structural disorder. However, for the $MoS_2$ grown on sulfur vapor

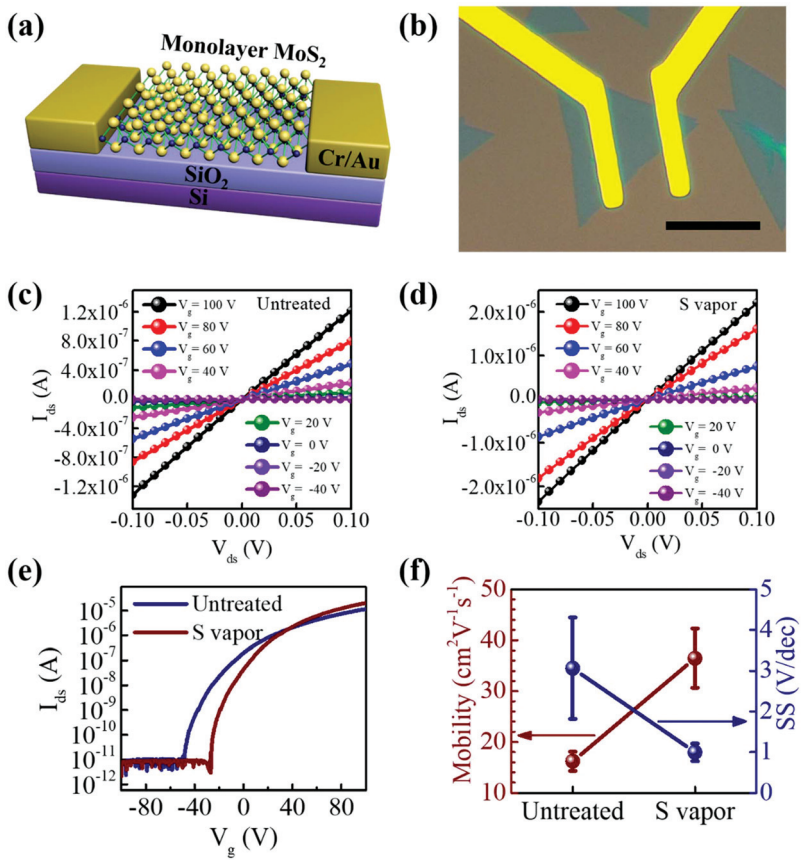


**Fig. 5** (a) Three-dimensional schematic of a monolayer $MoS_2$ transistor. (b) Optical image of a $MoS_2$ FET device. Scale bar, 20 μm. (c) Output characteristics of monolayer $MoS_2$ grown on untreated $SiO_2$/Si substrate. (d) Output characteristics of monolayer $MoS_2$ grown on sulfur vapor pretreated $SiO_2$/Si substrate. (e) Typical transfer characteristics of monolayer $MoS_2$ grown on sulfur vapor pretreated $SiO_2$/Si substrate (red line) and untreated $SiO_2$/Si substrate (blue line). (f) Statistical mobility and subthreshold swing of $MoS_2$ FET devices.

pretreated substrates, only a little enhancement in PL can be achieved, which indicates less defect-mediated nonradiative recombination in the as-grown $MoS_2$ before TFSI treatment. From TFSI repaired sulfur vacancy defects, the elimination of sulfur vacancy defects by TFSI is more obvious in $MoS_2$ grown on untreated substrates. We conclude that the density of sulfur vacancies is much lower in $MoS_2$ grown on sulfur vapor pretreated substrates.

Finally, we performed electrical characterization of the monolayer $MoS_2$ samples. Fig. 5(a) and (b) show the schematics and typical optical image of the $MoS_2$ transistor, respectively. Back-gated FET devices on the individual $MoS_2$ flakes were directly fabricated on the growth substrates without a further transfer process. The linear current–voltage ($I_{ds}$–$V_{ds}$) curves of $MoS_2$ flakes grown on both substrates indicate that the contact between $MoS_2$ and metal electrode is ohmic, as illustrated in Fig. 5(c) and (d). The transfer curves of $MoS_2$ FET devices in Fig. 5(e) show good n-type semiconducting behavior, which is consistent with earlier literature reports.[2,3,16–18] The on/off current ratio of the $MoS_2$ FET is about $10^6$–$10^7$. The mobility can be calculated based on the formula:

$$\mu = \frac{L}{W \times C_g \times V_{ds}} \times \frac{dI_{ds}}{dV_g}, \quad (1)$$

where $L$ and $W$ are the channel length and width, respectively, and $C_g$ is the capacitance ($C_g = 1.15 \times 10^{-8}$ F cm$^{-2}$) for 300 nm $SiO_2$. Multiple $MoS_2$ FET devices were tested, and the statistical results are shown in Fig. 5(f). The mobility of $MoS_2$ grown on untreated substrates ranged from 13–18.8 cm$^2$ V$^{-1}$ s$^{-1}$, whereas the mobility of $MoS_2$ grown on sulfur vapor pretreated substrates can be up to 40 cm$^2$ V$^{-1}$ s$^{-1}$ (as seen from Fig. 5(e), red line), which exceeds twice the value of that grown on untreated substrates. The mobility of monolayer $MoS_2$ grown on the sulfur vapor pretreated substrate is superior to most reported values of mechanically exfoliated monolayer $MoS_2$ and CVD grown monolayer $MoS_2$ without post-treatment (as shown in Fig. S7†). It should be noted that the mobility of up to 81 cm$^2$ V$^{-1}$ s$^{-1}$ of $MoS_2$ is on the precondition that both sides of $MoS_2$ should be treated with sulfur-containing molecules.[24] On the one hand, it is found that the statistic subthreshold swing (SS) of $MoS_2$ grown on untreated substrates is more than twice larger than that grown on sulfur vapor pretreated substrates, which means that the latter has reduced interface trap states and better crystal quality.[26] On the other hand, we found that the threshold voltage has an obvious negative shift in $MoS_2$ grown on untreated substrates compared with $MoS_2$ grown on sulfur vapor pretreated substrates, which means that the much heavier n-doping resulted from the higher density of sulfur vacancies in $MoS_2$ grown on untreated substrates.

## Conclusions

In summary, we demonstrate a simple and effective strategy to synthesize high quality monolayer $MoS_2$ by pretreating $SiO_2$/Si substrates with sulfur vapor. The optical responses of monolayer $MoS_2$ grown on sulfur vapor pretreated $SiO_2$/Si substrates are remarkably improved compared with those of monolayer $MoS_2$ grown on untreated $SiO_2$/Si substrates. Raman characterization and TFSI treatment confirm that $MoS_2$ grown on sulfur vapor pretreated substrates has a much lower density of sulfur vacancies. The carrier mobility of $MoS_2$ grown on sulfur vapor pretreated $SiO_2$/Si substrates reaches up to 40 cm$^2$ (V s)$^{-1}$ even at ambient temperature. Our work boosts the research on $MoS_2$ both in the fundamental studies and its further application in optoelectronics.

## Author contributions

Chunxiao Cong directed the research work. Chunxiao Cong and Peng Yang conceived and designed the experiments. Peng Yang fabricated the $MoS_2$ samples. Peng Yang and Yabing Shan performed the Raman and PL measurements. Peng Yang and Jing Chen fabricated the $MoS_2$ devices and performed the electrical performance measurements. Chunxiao Cong, Peng Yang, Haomin Wang, and Zhi-Jun Qiu analysed the data. Chunxiao Cong and Peng Yang co-wrote the manuscript. All authors discussed the results and commented on the manuscript.

## Conflicts of interest

There are no conflicts to declare.

## Acknowledgements

This work is supported by the National Key R&D Program of China (Grant No. 2018YFA0703700 and 2017YFF0206106), the National Natural Science Foundation of China (Grant No. 61774040, 61774042, and 51772317), the Shanghai Municipal Science and Technology Commission (Grant No. 18JC1410300), the Fudan University-CIOMP Joint Fund (Grant No. FC2018-002), the National Young 1000 Talent Plan of China, the Shanghai Municipal Natural Science Foundation (Grant No. 16ZR1402500, 16ZR1442700, 17ZR1446500, and 17ZR1446600), the "First-Class Construction" project of Fudan University (No. XM03170477) and the State Key Laboratory of ASIC & System, Fudan University (No. 2018MS001). Peng Yang thanks Yanqing Zhao, Yan Sun and Yao Guo from Beijing Institute of Technology for their useful discussion in the PL spectra section.

## References

1 S. B. Desai, S. R. Madhvapathy, A. B. Sachid, J. P. Llinas, Q. X. Wang, G. H. Ahn, G. Pitner, M. J. Kim, J. Bokor, C. M. Hu, H.-S. P. Wong and A. Javey, *Science*, 2016, **354**, 99–102.

 

2 Z. Y. Lin, Y. Liu, U. Halim, M. N. Ding, Y. Y. Liu, Y. L. Wang, C. C. Jia, P. Chen, X. D. Duan, C. Wang, F. Song, M. F. Li, C. Z. Wan, Y. Huang and X. F. Duan, *Nature*, 2018, **562**, 254–258.
3 B. Radisavljevic, A. Radenovic, J. Brivio, V. Giacometti and A. Kis, *Nat. Nanotechnol.*, 2011, **6**, 147–150.
4 C. S. Liu, H. W. Chen, X. Hou, H. Zhang, J. Han, Y.-G. Jiang, X. Y. Zeng, D. W. Zhang and P. Zhou, *Nat. Nanotechnol.*, 2019, **14**, 662–667.
5 M. Zhao, Y. Ye, Y. M. Han, Y. Xia, H. Y. Zhu, S. Q. Wang, Y. Wang, D. A. Muller and X. Zhang, *Nat. Nanotechnol.*, 2016, **11**, 954–959.
6 T. Roy, M. Tosun, J. S. Kang, A. B. Sachid, S. B. Desai, M. Hettick, C. C. Hu and A. Javey, *ACS Nano*, 2014, **8**, 6259–6264.
7 C. X. Cong, J. Z. Shang, Y. L. Wang and T. Yu, *Adv. Opt. Mater.*, 2018, **6**, 1700767.
8 A. D. Bartolomeo, F. Urban, M. Passacantando, N. McEvoy, L. Peters, L. Iemmo, G. Luongo, F. Romeo and F. Giubileo, *Nanoscale*, 2019, **11**, 1538–1548.
9 K. F. Mak, C. Lee, J. Hone, J. Shan and T. F. Heinz, *Phys. Rev. Lett.*, 2010, **105**, 136805.
10 A. Splendiani, L. Sun, Y. B. Zhang, T. S. Li, J. W. Kim, C.-Y. Chim, G. Galli and F. Wang, *Nano Lett.*, 2010, **10**, 1271–1275.
11 J.-B. Li, S. Xiao, S. Liang, M.-D. He, N.-C. Kim, Y. F. Luo, J.-H. Luo and L.-Q. Chen, *Opt. Express*, 2017, **25**, 13567–13576.
12 J. Z. Shang, C. X. Cong, L. S. Wu, W. Huang and T. Yu, *Small Methods*, 2018, **2**, 1800019.
13 H. L. Zeng, J. F. Dai, W. Yao and X. D. Cui, *Nat. Nanotechnol.*, 2012, **7**, 490–493.
14 O. Lopez-Sanchez, D. Lembke, M. Kayci, A. Radenovic and A. Kis, *Nat. Nanotechnol.*, 2013, **8**, 497–501.
15 S. Hussain, J. Singh, D. Vikraman, A. K. Singh, M. Z. Iqbal, M. F. Khan, P. Kumar, D.-C. Choi, W. Song, K.-S. An, J. Eom, W.-G. Lee and J. Jung, *Sci. Rep.*, 2016, **6**, 30791.
16 Y.-H. Lee, X.-Q. Zhang, W. J. Zhang, M.-T. Chang, C.-T. Lin, K.-D. Chang, Y.-C. Yu, J. T.-W. Wang, C.-S. Chang, L.-J. Li and T.-W. Lin, *Adv. Mater.*, 2012, **24**, 2320–2325.
17 P. F. Yang, X. L. Zou, Z. P. Zhang, M. Hong, J. P. Shi, S. L. Chen, J. P. Shu, L. Y. Zhao, S. L. Jiang, X. B. Zhou, Y. H. Huan, C. Y. Xie, P. Gao, Q. Chen, Q. Zhang, Z. F. Liu and Y. F. Zhang, *Nat. Commun.*, 2018, **9**, 979.
18 K. Kang, S. E. Xie, L. J. Huang, Y. M. Han, P. Y. Huang, K. F. Mak, C.-J. Kim, D. Muller and J. Park, *Nature*, 2015, **520**, 656–660.
19 P. Yang, A.-G. Yang, L. X. Chen, J. Chen, Y. W. Zhang, H. M. Wang, L. G. Hu, R.-J. Zhang, R. Liu, X.-P. Qu, Z.-J. Qiu and C. X. Cong, *Nano Res.*, 2019, **12**, 823–827.
20 W. Zhou, X. L. Zou, S. Najmaei, Z. Liu, Y. M. Shi, J. Kong, J. Lou, P. M. Ajayan, B. I. Yakobson and J.-C. Idrobo, *Nano Lett.*, 2013, **13**, 2615–2622.
21 A. Zafar, H. Y. Nan, Z. Zafar, Z. T. Wu, J. Jiang, Y. M. You and Z. H. Ni, *Nano Res.*, 2017, **10**, 1608–1617.
22 K. Wu, Z. Li, J. B. Tang, X. L. Lv, H. L. Wang, R. C. Luo, P. Liu, L. H. Qian, S. P. Zhang and S. L. Yuan, *Nano Res.*, 2018, **11**, 4123–4132.
23 S. Roy, W. Choi, S. Jeon, D.-H. Kim, H. Kim, S. J. Yun, Y. J. Lee, J. Lee, Y.-M. Kim and J. Kim, *Nano Lett.*, 2018, **18**, 4523–4530.
24 Z. H. Yu, Y. M. Pan, Y. T. Shen, Z. L. Wang, Z.-Y. Ong, T. Xu, R. Xin, L. J. Pan, B. G. Wang, L. T. Sun, J. L. Wang, G. Zhang, Y. W. Zhang, Y. Shi and X. R. Wang, *Nat. Commun.*, 2014, **5**, 5290–5296.
25 M. Amani, R. A. Burke, X. Ji, P. D. Zhao, D.-H. Lien, P. Taheri, G. H. Ahn, D. Kirya, J. W. Ager III, E. Yablonovitch, J. Kong, M. Dubey and A. Javey, *ACS Nano*, 2016, **10**, 6535–6541.
26 M. Amani, D.-H. Lien, D. Kiriya, J. Xiao, A. Azcatl, J. Noh, S. R. Madhvapathy, R. Addou, S. KC, M. Dubey, K. Cho, R. M. Wallace, S.-C. Lee, J.-H. He, J. W. Ager III, X. Zhang, E. Yablonovitch and A. Javey, *Science*, 2015, **350**, 1065–1068.
27 K. Cho, M. Min, T.-Y. Kim, H. Jeong, J. Pak, J.-K. Kim, J. Jang, S. J. Yun, Y. H. Lee, W.-K. Hong and T. Lee, *ACS Nano*, 2015, **9**, 8044–8053.
28 M. Makarova, Y. Okawa and M. Aono, *J. Phys. Chem. C*, 2012, **116**, 22411–22416.
29 X. K. Zhang, Q. L. Liao, S. Liu, Z. Kang, Z. Zhang, J. L. Du, F. Li, S. H. Zhang, J. K. Xiao, B. S. Liu, Y. Ou, X. Z. Liu, L. Gu and Y. Zhang, *Nat. Commun.*, 2017, **8**, 15881.
30 H. Y. Nan, Z. L. Wang, W. H. Wang, Z. Liang, Y. Lu, Q. Chen, D. W. He, P. H. Tan, F. Miao, X. R. Wang, J. L. Wang and Z. H. Ni, *ACS Nano*, 2014, **8**, 5738–5745.
31 F. Urban, F. Giubileo, A. Grillo, L. Iemmo, G. Luongo, M. Passacantando, T. Foller, L. Madauß, E. Pollmann, M. P. Geller, D. Oing, M. Schleberger and A. D. Bartolomeo, *2D Mater.*, 2019, **6**, 045049.
32 H. L. Wang, C. J. Zhang and F. Rana, *Nano Lett.*, 2014, **15**, 339–345.
33 K. M. McCreary, A. T. Hanbicki, S. V. Sivaram and B. T. Jonker, *APL Mater.*, 2018, **6**, 111106.
34 H. Jeong, H. M. Oh, A. Gokarna, H. Kim, S. J. Yun, G. H. Han, M. S. Jeong, Y. H. Lee and G. Lerondel, *Adv. Mater.*, 2017, **29**, 1700308.
35 L. Fu, Y. Y. Sun, N. Wu, R. G. Mendes, L. F. Chen, Z. Xu, T. Zhang, M. H. Rümmeli, B. Rellinghaus, D. Pohl, L. Zhuang and L. Fu, *ACS Nano*, 2016, **10**, 06254.
36 A. M. Yan, J. V. Jr, S. Kahn, K. Watanabe, T. Taniguchi, F. Wang, M. F. Crommie and A. Zettl, *Nano Lett.*, 2015, **15**, 6324–6331.
37 A. M. van der Zande, Y. M. You, G.-H. Lee, T. F. Heinz, D. R. Reichman, D. A. Muller, J. C. Hone, P. Y. Huang, D. A. Chenet and T. C. Berkelbach, *Nat. Mater.*, 2013, **12**, 554–561.
38 J. Z. Shang, X. N. Shen, C. X. Cong, N. Peimyoo, B. C. Cao, M. Eginligil and T. Yu, *ACS Nano*, 2015, **9**, 647–655.
39 V. Carozo, Y. X. Wang, K. Fujisawa, B. R. Carvalho, A. McCreary, S. M. Feng, Z. Lin, C. J. Zhou, N. Perea-López, A. L. Elías, B. Kabius, V. H. Crespi and M. Terrones, *Sci. Adv.*, 2017, **3**, 1602813.

40 L. Xu, L. Y. Zhao, Y. S. Wang, M. C. Zou, Q. Zhang and A. Y. Cao, *Nano Res.*, 2019, **12**, 1619–1624.
41 R. Rao, V. Carozo, Y. X. Wang, A. E. Islam, N. Perea-Lopez, K. Fujisawa, V. H. Crespi, M. Terrones and B. Maruyama, *2D Mater.*, 2019, **6**, 045031.
42 X. Zhang, X.-F. Qiao, W. Shi, J.-B. Wu, D.-S. Jiang and P.-H. Tan, *Chem. Soc. Rev.*, 2015, **44**, 2757–2785.
43 M. G. Sensoy, D. Vinichenko, W. Chen, C. M. Friend and E. Kaxiras, *Phys. Rev. B*, 2017, **95**, 014106.
44 H. Yu, Z. Z. Yang, L. J. Du, J. Zhang, J. N. Shi, W. Chen, P. Chen, M. Z. Liao, J. Zhao, J. L. Meng, G. L. Wang, J. Q. Zhu, R. Yang, D. X. Shi, L. Gu and G. Y. Zhang, *Small*, 2016, **13**, 1603005.
45 I. S. Kim, V. K. Sangwan, D. Jariwala, J. D. Wood, S. Park, K.-S. Chen, F. Y. Shi, F. Ruiz-Zepeda, A. Ponce, M. Jose-Yacaman, V. P. Dravid, T. J. Marks, M. C. Hersam and L. J. Lauhon, *ACS Nano*, 2014, **8**, 10551–10558.
46 R. X. Wang, D. J. Zhang and C. B. Liu, *Chem. Phys. Lett.*, 2005, **404**, 237–243.
47 J. Roche, P. Ryan and G. Hughes, *Surf. Sci.*, 2000, **465**, 115–119.
48 T. Hahn, H. Metzner, H. B. Plikat and M. Seibt, *Appl. Phys. Lett.*, 1998, **72**, 2733–2735.
49 H. Metzner, T. Hahn, J.-H. Breme and J. Conrad, *Appl. Phys. Lett.*, 1996, **69**, 1900–1902.